ACS APPLIED POLYMER MATERIALS

pubs.acs.org/acsapm Article

Thermally Reprocessable Self-Healing Single-Ion Conducting Polymer Electrolytes

Sangho Lee,[#] Juhwan Song,[#] Jinhan Cho, Jeong Gon Son,* and Tae Ann Kim*

Cite This: ACS Appl. Polym. Mater. 2023, 5, 7433−7442 Read Online

ACCESS | Metrics & More | Article Recommendations | Supporting Information

ABSTRACT: Self-healing polymer electrolytes are essential for overcoming the limitations of liquid and solid electrolytes by offering superior mechanical robustness, enhanced safety, and repeated processability. Herein, we present thermally reprocessable and self-healing thermosets for solid polymer electrolytes using sulfonylimide-based anionic monomers and thermo-reversible Diels−Alder chemistry. Six different types of linear copolymers are synthesized by varying the chemical structures of furan-containing monomers and the proportion of electrolytic components. Then, bismaleimide cross-linkers are introduced to form thermally reversible cross-linked networks. We investigate the effect of the comonomer ratio and monomer structure on the thermomechanical and electrochemical properties of these polymers. Furthermore, we evaluate the mechanical and ion conducting properties after up to 30 thermal reprocessing cycles. Our findings demonstrate the potential of these thermosets as promising candidates for high-performance solid polymer electrolytes in lithium-ion batteries.

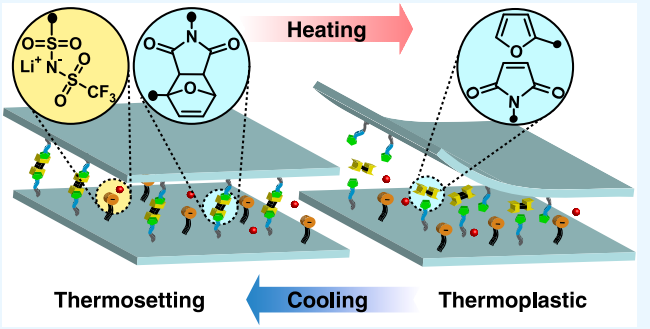

KEYWORDS: *polymer electrolytes, single-ion conducting membranes, recyclable thermosets, sustainable polymers, self-healing*

1. INTRODUCTION

Electrolytes play a crucial role in facilitating the movement of ions between electrodes, making them essential components for batteries,[1] fuel cells,[2,3] and other electrochemical devices.[4,5] While liquid electrolytes are widely used because of their high ionic conductivity, they become volatile at higher temperatures and possess flammability risks. Moreover, devices using liquid electrolytes tend to be bulkier and require extra space. As potential alternatives to replace liquid electrolytes, solid polymer electrolytes (SPEs) emerge as highly sought-after candidates since they have excellent stability, low cost, and ease of fabrication.[6−8] Particularly in lithium-ion batteries (LIBs), the use of SPEs can reduce the formation of lithium dendrites in the anodes, which is closely related to safety concerns associated with LIBs.[9−11]

When designing ion conducting polymers for solid electrolytes, polymer electrolytes need to be mechanically durable to serve as both the electrolyte and separator.[12] Typically, chemically cross-linked thermosetting polymers are used owing to their high mechanical and chemical stabilities, but they are not compatible with current manufacturing methods for large-scale production of electrochemical devices such as slurry casting and roll-to-roll technologies.[13] As the proper recycling of electrochemical devices has become increasingly important at the end of their lifespan for future sustainability consideration,[14] it is crucial to develop recyclable polymer electrolytes that possess excellent mechanical properties and reprocessability while retaining their properties. Furthermore, their self-healing and robust characteristics enable them to compensate for volume changes in the electrodes through elastic and plastic deformation, providing additional safety.[15,16]

Dynamic covalent chemistry, which combines the stability of covalent bonds with the reversibility of noncovalent bonds, is a powerful tool for designing chemically recyclable and self-healing polymers.[17,18] Commonly, gel polymer electrolytes have been prepared by mixing a dynamic covalent polymer with some additives. The polymer matrix provides the self-healing and chemical recycling function, and the additives such as plasticizers with lithium salts facilitate the transport of lithium ions.[19,20] Some ionic liquids (ILs) have been used as suitable plasticizers such as 1-ethyl-3-methylimidazolium bis(trifluoromethylsulfonyl)imide ([EMIM][TFSI]), due to their good ionic conductivity and electrochemical stability.[21] However, a high amount of the plasticizer can impair the thermal stability, reduce the mechanical strength, and most importantly increase the risk of safety hazards. Additionally, for those binary salts, both lithium ions and their counteranions

Received: June 19, 2023
Accepted: August 1, 2023
Published: August 16, 2023

Scheme 1. Schematic of Thermally Reprocessable and Self-Healing Polymer Electrolytes

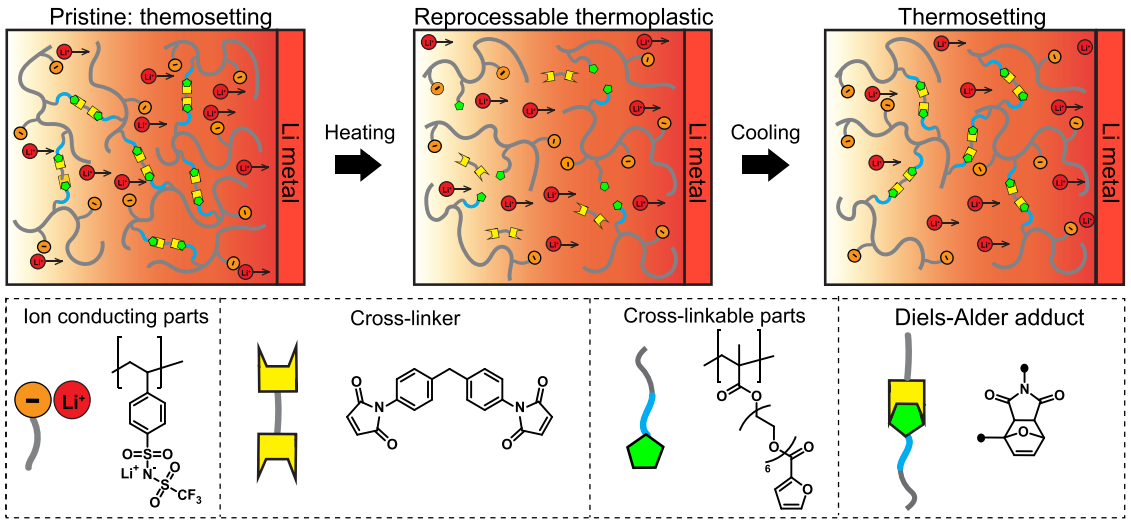

migrate between electrodes during the charging and discharging process.[22] Since the conductivity of binary salt conductors is dominated by the motion of anions, the fraction of current carried by lithium ions (t_{Li^+}) is relatively low. The accumulation of anions at the interfaces between the electrode and electrolyte also causes power loss in the battery. Therefore, the free movement of anions needs to be limited or eliminated by covalently attaching anions to the backbone chains of the host polymers to form single-ion conductors.[23]

Ion conduction in polymer electrolytes is strongly correlated with the local segmental motion of the polymers.[24,25] As a result, solid-state single-ion conductors have been mainly made using polymers with a low glass transition temperature (T_g), such as poly(ethylene oxide) (PEO). The PEO units possess good donor ability for lithium ions and high chain flexibility, which are crucial for facilitating lithium-ion transport. For instance, incorporating PEO units into the backbone or grafting as side chains of polymer electrolytes significantly increased the diffusivity and ionic conductivity of the lithium ion compared to the electrolytes without PEO units.[26] Furthermore, numerous strategies have been reported to enhance the ionic conductivity of polymer electrolytes. These approaches include controlling phase-separated morphologies,[27,28] altering anionic structures,[29−32] engineering side chains,[33] and incorporating additives.[34]

Herein, we demonstrate thermally recyclable and single-ion conducting thermosets for SPEs using sulfonylimide-based anionic monomers and thermo-reversible DA chemistry (Scheme 1.). Linear random copolymers are synthesized with lithium 4-styrenesulfonyl(trifluoromethylsulfonyl)imide (LiSTFSI) and furan-containing monomers. Two types of furan-containing monomers are incorporated to investigate the effect of EO moieties for the conductivity of the lithium ion: furfuryl methacrylate and poly(ethylene glycol) methacrylate (PEGMA, M_n = 360 g mol^{-1}) terminated with a furan group. Then, bismaleimide cross-linkers are mixed with the linear polymers to prepare thermo-reversible cross-linked networks. We investigated the effect of the comonomer ratio and monomer structure on thermomechanical and electrochemical properties. Furthermore, the mechanical and ion conducting properties are evaluated after multiple recycling processes.

2. EXPERIMENTAL SECTION

2.1. Materials. Unless otherwise stated, all reagents were purchased from a commercial source and used as received. Sodium 4-vinylbenzenesulfonate (≥90%, Sigma-Aldrich) and azobis(2-methylpropionitrile) (AIBN) were recrystallized in anhydrous ethanol/distilled water (9:1, v/v) and methanol, respectively. Polyethylene glycol methacrylate (PEGMA, M_n = 360 g mol^{-1}, Sigma-Aldrich) and furfuryl methacrylate (FMA, 97%, Sigma-Aldrich) were passed through a column of basic alumina to remove inhibitors. The PEGMA was further dried overnight in a vacuum oven at 30 °C prior to use.

2.2. Synthesis of Lithium (4-Styrenesulfonyl)-(trifluoromethanesulfonyl)imide (LiSTFSI). LiSTFSI was synthesized following the previous studies with some modification (Scheme S1).[35,36] Anhydrous acetonitrile (15 ml) and dimethylformamide (DMF, 0.25 ml) were added into a round-bottom flask. Oxalyl chloride (0.86 ml, 0.01 mol, 1 equiv) was mixed with the solvent and stirred for 1 h at room temperature. Sodium 4-vinylbenzenesulfonate (2.1 g, 0.01 mol, 1 equiv) was added to the solution at 0 °C and stirred for 2 h, followed by further stirring for 3 h at room temperature. Then, trifluoromethanesulfonamide (1.5 g, 0.01 mol, 1 equiv) and trimethylamine (0.88 ml, 0.01 mol, 1 equiv) were injected and stirred for 30 min at 0 °C. After 30 min, the solution was stirred overnight at room temperature. The solvent was completely removed and washed with dichloromethane, 4 wt % $NaHCO_3$ solution, and 1 M HCl. After that, the organic layer was collected and dried in a vacuum oven. The resulting product was dissolved in 20 ml of DI water, and LiOH (0.63 g, 0.015 mol, 1.5 equiv) was added. The solution was stirred overnight, filtered to remove excess lithium salt, and dried in a vacuum (2.8 g, 8.9 mmol, 87%). The characterization data are provided in the Supporting Information (Figure S1).

2.3. Synthesis of Furan-Terminated Polyethylene Glycol Methacrylate (PEGFMA). PEGFMA was prepared according to literature procedures (Scheme S2).[37] Dichloromethane (DCM, 20 ml) and PEGMA (3.6 g, 0.01 mol, 1 equiv) were injected in an Ar-purged round-bottom flask. Then, 2-furoyl chloride (1.0 ml, 0.01 mol, 1 equiv) was added with additional DCM (10 ml). After the mixture was cooled to 0 °C in an ice bath, pyridine (0.80 ml, 0.01 mol, 1 equiv) was injected dropwise and stirred for 24 h at room temperature. Once the reaction was completed, the mixture was washed with water several times. The organic layer was collected, and the solvent was evaporated, resulting in a viscous yellow liquid (4.2 g, 9.2 mmol, 92%). The characterization data are provided in the Supporting Information (Figure S2).

2.4. Synthesis of Poly(LiSTFSI-*co*-FMA) and Poly(LiSTFSI-*co*-PEGFMA). Three types of poly(LiSTFSI-*co*-FMA) (**L**) and poly(LiSTFSI-*co*-PEGFMA) (**LP**) were synthesized by changing the

https://doi.org/10.1021/acsapm.3c01319
ACS Appl. Polym. Mater. 2023, 5, 7433−7442

Scheme 2. Synthetic Scheme for (a) Ls and (b) LPs

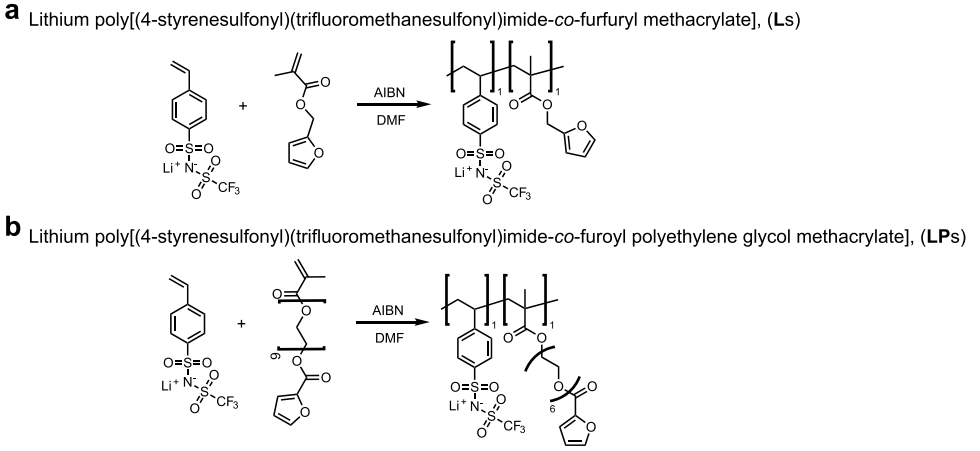

molar contents of furan-containing monomers (Scheme 2). The molecular weight, molar content of FMA or PEGFMA, and thermal stabilities of each polymer are summarized in Table 1. The molar content of LiSTFSI (electrolytic part) increases with each sample number.

Table 1. Poly(LiSTFSI-*co*-FMA) (L) and Poly(LiSTFSI-*co*-PEGFMA) (LP) Synthesized in This Study

sample	M_n (kg mol^{-1})	$Đ$	electrolyte ratio	$T_{5\%}$ (°C)
L1	7.5	2.45	0.49	153
L2	6.6	2.48	0.65	325
L3	13	2.22	0.85	429
LP1	11	2.48	0.45	171
LP2	9.8	2.35	0.70	298
LP3	8.3	2.23	0.90	379

The polymerization procedure used for **LP3** proceeded as follows. Anhydrous DMF (20 ml) was injected in an Ar-purged round-bottom flask and heated to 60 °C. AIBN (0.022 g, 0.013 mmol, 1.0 equiv) was dissolved in anhydrous DMF (5 ml) and injected to the flask. After stirring for 10 min, the solution of LiSTFSI (1.3 g, 3.9 mmol, 300 equiv) and PEGFMA (0.16g, 0.35 mmol, 27 equiv) dissolved in anhydrous DMF (5 ml) was added. The mixture was stirred for 24 h at 60 °C. The polymer was precipitated in anhydrous diethyl ether (300 ml) and dried under vacuum. The dried product was redissolved in deionized water (20 ml), followed by dialysis against distilled water using a dialysis membrane (cutoff molecular weight = 2 kDa). Finally, the polymer solution was freeze-dried to obtain a yellow powder. The characterization data are provided in the Supporting Information (Figures S3–S8).

2.5. Preparation of Thermally Recyclable and Single-Ion Conducting Thermosets. Each linear polymer was dissolved in anhydrous DMF (5 ml). Then, 4,4′-bismaleimidodiphenylmethane was added at an equivalent molar ratio to the furan functional groups present in the polymer. The mixture was stirred for 10 min and poured onto a Teflon plate. The solution was dried overnight in a vacuum oven at 70 °C to get cross-linked polymers (**xLs** and **xLPs**).

2.6. Characterization. ^{1}H NMR, ^{13}C NMR, and ^{19}F NMR spectra were measured with DMSO-d_6 as the solvent (400 MHz, Bruker Avance 400 Ultrashield, Bruker). Spectra were referenced to the residual solvent peaks (^{1}H NMR: 2.50 ppm, ^{13}C NMR: 39.51 ppm). The molecular weights of linear polymers were characterized by gel permeation chromatography (GPC, Ultimate 3000, Thermofisher Scientific) with water as an eluent at 25 °C. Pullulan standards were used for molecular weight calibration. Fourier transform infrared spectra (FT-IR, 3 MIR FT-IR Spectrometer, PerkinElmer) were recorded over the range 550–4000 cm^{-1}. The thermal stability of linear polymers was measured by thermogravimetric analysis (TGA, Q50, TA Instrument) from 25 to 900 °C at a heating rate of 10 °C min^{-1}. Differential scanning calorimetry (DSC, DSC 4000, PerkinElmer) analyses were performed from 25 to 180 °C with a heating rate of 2 °C min^{-1} under a nitrogen atmosphere. Bar-shaped specimens (20 × 10 × 5.0 mm) were prepared, and uniaxial tensile tests were performed using a dynamic mechanical analyzer (DMA, Q800, TA Instruments) at a speed of 5 mm min^{-1}. At least five samples were tested, and average values with standard deviation were calculated. Rheological properties were determined with a rotational rheometer (MCR 302, Anton Parr, Austria). The samples were trimmed to a 25 mm diameter and placed between plates with a 0.5 mm gap. The frequency, strain, and temperature ranges were set at 1 Hz, 0.5%, and −20 to 180 °C, respectively. The stress–relaxation behavior of **xLPs** with **xLs** as a function of temperature was measured to determine the relaxation activation energy (E_a) for rDA reaction. The relaxation modulus was derived based on the Maxwell model

$$G(t) = G_0 e^{(-t/\tau)} \tag{1}$$

where $G(t)$, G_0, and t are the relaxation modulus, initial modulus, and time, respectively. τ is the characteristic relaxation time, which is defined at the time when $G(t)/G_0$ equals 1/e. Since τ^* follows the Arrhenius law, the following equation can be used to calculate the E_a.[38]

$$\ln \tau^* = \ln \tau_0 + \frac{E_a}{RT} \tag{2}$$

2.7. Electrochemical Properties. The ionic conductivity of all samples was determined by electrochemical impedance spectroscopy (EIS) on an electrochemical workstation (Autolab, Metrohm, Swiss) at a constant temperature (40, 50, 60, 70, and 80 °C). The frequency range was from 0.1 to 10^6 Hz with an AC potential amplitude of 5 mV. The ionic conductivity was calculated according to the following equation (eq 3)

$$\sigma = \frac{D}{R_b S} \tag{3}$$

where D is the distance between two stainless-steel electrodes and S is the contact area between the polymer membrane and the electrodes. The bulk resistance (R_b) was obtained from the Nyquist plot at the fitting model. The electrochemical stability window of samples was measured at room temperature using linear sweep voltammetry (LSV). A cell was assembled by sandwiching the polymer membrane between two stainless-steel disks, and the measurement was carried out from 0 to 7.8 V at a scanning rate of 1.0 mV s^{-1}. The $t_{Li}{}^+$ of the electrolytes was evaluated according to the method proposed by Abraham et al.[39] A membrane cell was assembled with stainless-steel electrodes, and a small polarization potential (ΔV) of 10 mV was applied to record the initial current (I_0) and the steady-state current (I_{SS}) at room temperature. Meanwhile, electrochemical impedance

https://doi.org/10.1021/acsapm.3c01319
ACS Appl. Polym. Mater. 2023, 5, 7433–7442

spectroscopy was performed to examine the initial and steady-state values of the interfacial resistances (R_{I0}, R_{ISS}) and the bulk resistances (R_{b0}, R_{bSS}) before and after polarization by applying a 5 mV amplitude between 10^5 and 10^{-1} Hz. The t_{Li}^+ was determined using eq 4

$$t_{Li}^+ = \frac{I_{SS}R_{bSS}(\Delta V - I_0R_{I0})}{I_0R_{b0}(\Delta V - I_{SS}R_{ISS})} \quad (4)$$

3. RESULTS AND DISCUSSION

3.1. Characterization of Linear Copolymers. Two types of linear single-ion conducting polymers (**L**s and **LP**s) were synthesized by free-radical polymerization, and their chemical structures were analyzed by ^{1}H NMR spectra (Figures 1, S3–S8). The successful incorporation of LiSTFSI and PEGFMA into **LP3** was confirmed by the presence of proton peaks corresponding to the backbone units (a, g), the benzene ring of the electrolyte units (b, c), and the furan ring and PEO chain from the cross-linking units (d, e, f). To determine the monomer composition, we used the integrated areas of the peaks from panels (c) and (e) due to the overlap of furan and styrene peaks for both polymers. The composition of copolymers matched the monomer feed ratio, and we synthesized three copolymers with a molecular weight of 10 kg mol^{-1}, varying the mole ratio of electrolytes: 90, 70, and 50 mol % (Table 1).

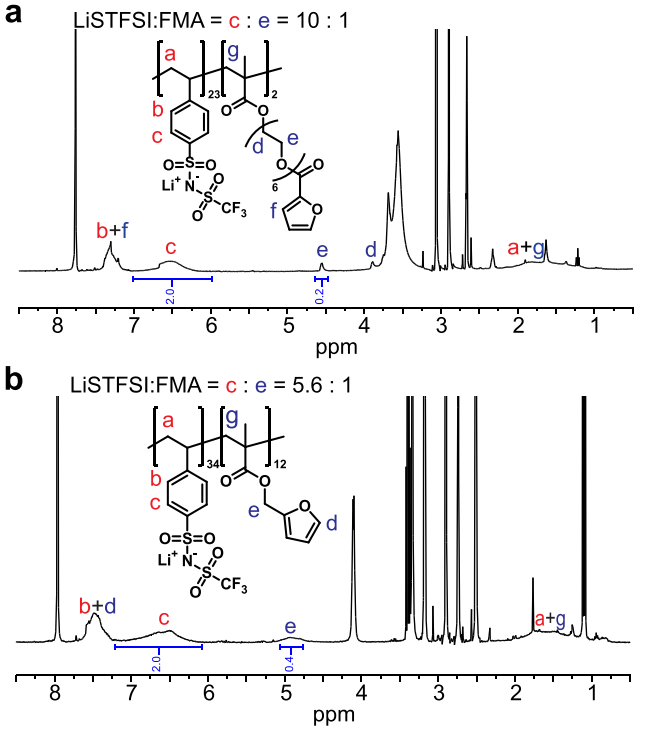

Figure 1. Chemical structures of polymers synthesized in this study. ^{1}H-NMR spectra of (a) **LP3** and (b) **L3**.

The thermal stability of the synthesized copolymers was characterized using TGA (Figure S9, Table 1). As the fraction of cross-linking parts increased, the onset temperature of thermal decomposition decreased. This can be attributed to the decomposition of FMA moieties into furfuryl alcohol at temperature ranging from 200 to 250 °C. Certain poly(FMA) can be converted into stable poly(cyclic anhydride) compounds, which remain intact up to 340 °C. Above 400 °C, the polymer starts to be decomposed again.[40] Therefore, polymers with a higher content of FMA or PEGFMA units (**L1** and **LP1**) exhibited a clear two-step decomposition behavior.

3.2. Thermo-Reversibility of Lithium-Ion Conducting Cross-Linked Polymers. Thermo-reversible cross-linked polymers were prepared by dissolving **L** or **LP** and cross-linkers in organic solvents and casting the solution onto a heated plate. The formation of the DA adducts was confirmed by their FT-IR spectra (Figure 2a). Following the addition of bismaleimide cross-linkers, characteristic peaks were observed, including those for the C—H bonds of C=C (700 cm^{-1}) and C=O carbonyl groups (1700 cm^{-1}) in the maleimide rings (**LP3** + cross-linker).[41] After the DA reaction was completed (**xLP3**), new absorption peaks appeared for C–O–C ether stretching vibrations (1070 cm^{-1}) and C=C double bond stretching vibrations (1774 cm^{-1}) of the DA adduct.

Generally, there are two types of DA adducts, thermally less stable *endo* and more stable *exo* adducts (Scheme S3), which are thermally dissociated above 100 °C via a retro DA reaction (rDA).[42] When maleimides are used for DA reaction, the *endo* form is known to be preferred due to their electron-withdrawing effect. During the first heating cycle of **xLP**s, we observed endothermic regions from 100 to 160 °C and the center of the peak at around 120 °C, implying that *endo* adducts were dominant (Figure 2b). As the molar content of furan increased, the endothermic region expanded toward higher temperatures. When each polymer was fully cured with the cross-linkers, the heat of the endothermic reaction (ΔH) for **xLP3**, **xLP2**, and **xLP1** was 3.9, 10.8, and 17.3 J g^{-1}, respectively. Based on the ΔH value of the furan-bismaleimide Diels–Alder reaction (43 ± 11 kJ mol^{-1}),[43] the degree of cross-linking for **xLP**s was determined to be 34±4%. When subjecting the cross-linked polymers to swell in DMF, we did not observe any mass change, indicating that all of the cross-linkers had successfully reacted with the terminal furan groups (Table S1).

Solubility tests were conducted to confirm the thermo-reversible cross-linking/de-cross-linking reactions in good solvents for linear polymers and cross-linkers such as dimethylformamide (Figure 2c). The cross-linked polymers were slightly swelled in dimethylformamide at room temperature but fully dissolved at temperatures above 130 °C. After removing all of the solvents, the residual polymers were attempted to be redissolved in dimethylformamide, but they were unable to dissolve, indicating that the DA reaction had proceeded. The resulting polymer exhibited reversible changes in solubility with temperature.

3.3. Thermomechanical and Tensile Properties of xLs and xLPs. The thermomechanical properties of **xL**s and **xLP**s were analyzed using dynamic mechanical analyses (DMA) in tension mode (Figure 3a,b). As the molar content of the furan-containing monomer increased (from **3** to **1**), the storage moduli in the glassy and rubbery regions increased for both samples. This suggests that the material became more elastic due to the increased number of cross-linking moieties. Unlike conventional cross-linked polymers showing constant storage moduli in the rubbery regions,[44] our polymers exhibited a decrease in the modulus above 100 °C due to the dissociation of cross-linking networks from the rDA reaction. Although our cross-linked polymers undergo changes in the modulus with temperature, their modulus values are high enough to suppress the dendrite growth within the operation temperature for LIBs (−20 to 60 °C).[45−47] Furthermore, the storage modulus of our

https://doi.org/10.1021/acsapm.3c01319
ACS Appl. Polym. Mater. 2023, 5, 7433−7442

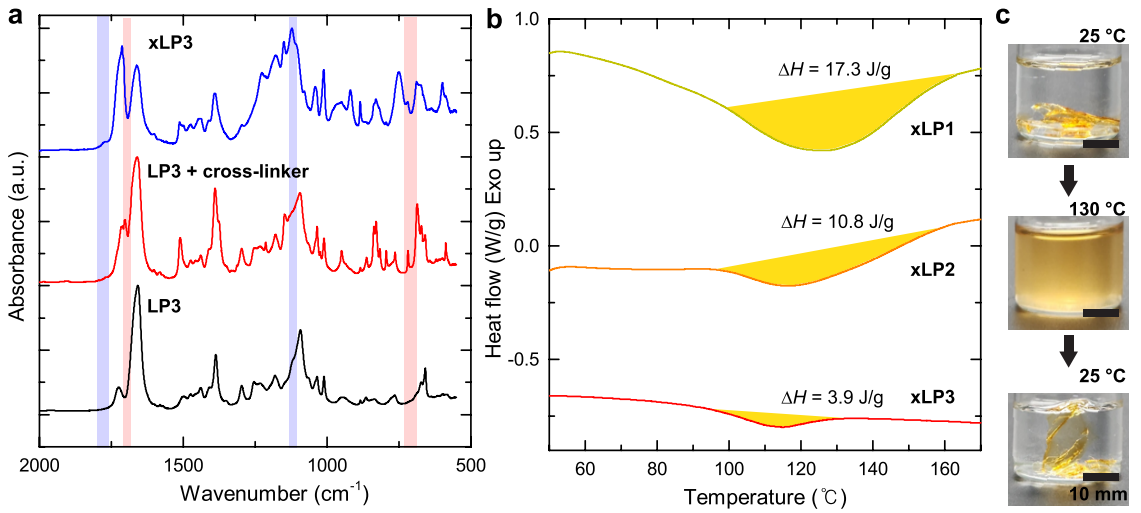

Figure 2. Formation of thermo-reversible cross-linked networks. (a) FT-IR results of the single-ion conducting linear polymer (**LP3**, black line), **LP3** with cross-linkers immediately after mixing (before DA reaction, red line), and after the DA reaction was completed (**xLP3**, blue line). (b) DSC results of **xLP1**, **xLP2**, and **xLP3** during the first heating cycle. (c) Digital images of **xLP3** in DMF at different temperatures.

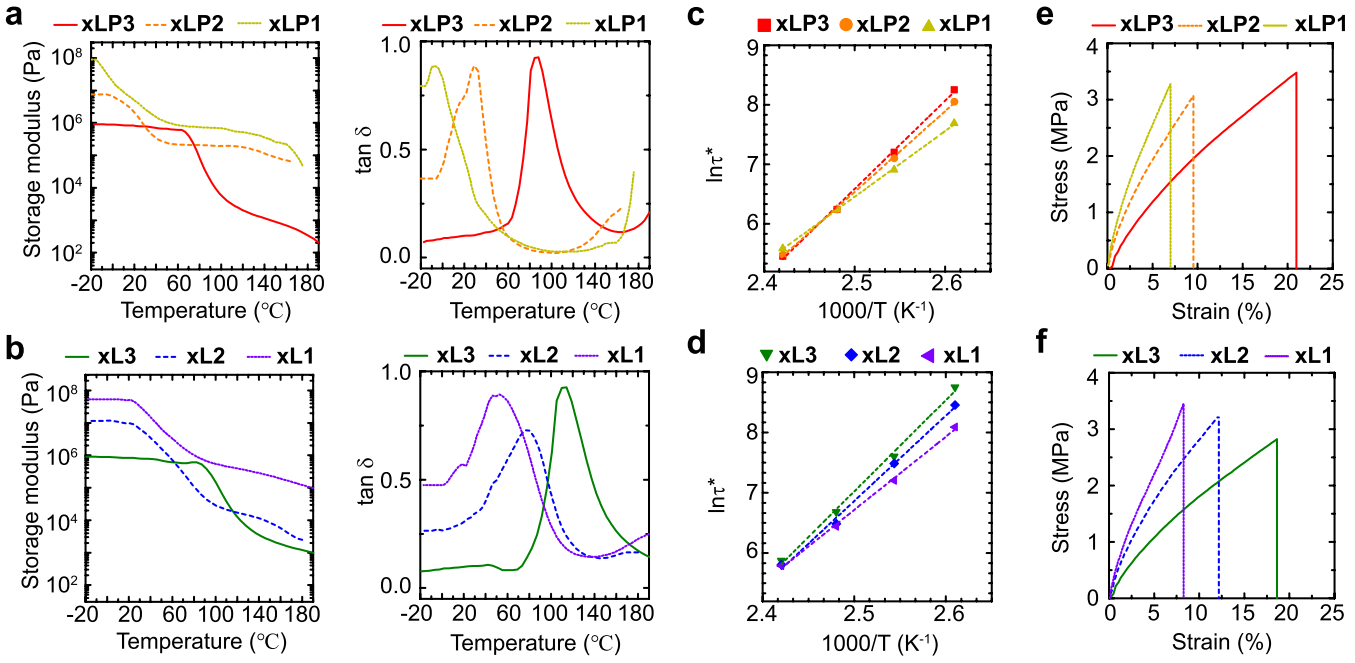

Figure 3. Thermomechanical and tensile properties of **xLs** and **xLPs**. Storage modulus and tan δ values of (a) **xLPs** and (b) **xLs**. Arrhenius plots obtained from τ^* at different temperatures of (c) **xLPs** and (d) **xLs**. The activation energy (E_a) for the rDA reaction was calculated from a linear fit (dashed line). Engineering stress−strain curves of (e) **xLPs** and (f) **xLs**.

polymers is at least two times higher than that of PEO-based copolymer electrolytes.[48]

The change in glass transition temperature (T_g) with the comonomer type and ratio was observed by tan δ values with temperature. The T_g values increased with the electrolytic parts (from **1** to **3**) for both **xLs** and **xLPs**. Particularly, **xLPs** containing the PEO units had a lower T_g than **xLs** with the same electrolyte content. This finding is consistent with the observed trend of T_g values for homopolymers of poly(LISTSFI), poly(FMA), and poly(PEGFMA), which are 256, 57, and −50 °C, respectively.[49−51]

The stress relaxation behaviors of **xLs** and **xLPs** were measured as a function of temperature to determine the activation energy (E_a) of the rDA reaction (Figure 3c,d). The relaxation time was determined by applying Maxwell's model when the ratio of shear modulus ($G(t)$) to the initial shear modulus (G_0) reached 1/e at each temperature (Figure S10).[38] Then, the values of E_a of the rDA reaction were calculated from the Arrhenius equation, resulting in 123, 113, and 92 kJ mol^{-1} (**xLP3**, **xLP2**, and **xLP1**) and 126, 118, and 101 kJ mol^{-1} (**xL3**, **xL2**, and **xL1**). Based on the previous literature, polymers with a higher mobility, as indicated by those with lower T_g and less cross-linking points, tend to facilitate the reversible process of the DA reaction at lower temperatures with faster rates.[52] Both samples exhibited an increase in the E_a value as the proportion of poly(LISTSFI) increased, possibly due to reduced chain mobility resulting from higher amounts of the polymers with a high T_g. This could impede the

https://doi.org/10.1021/acsapm.3c01319
ACS Appl. Polym. Mater. 2023, 5, 7433−7442

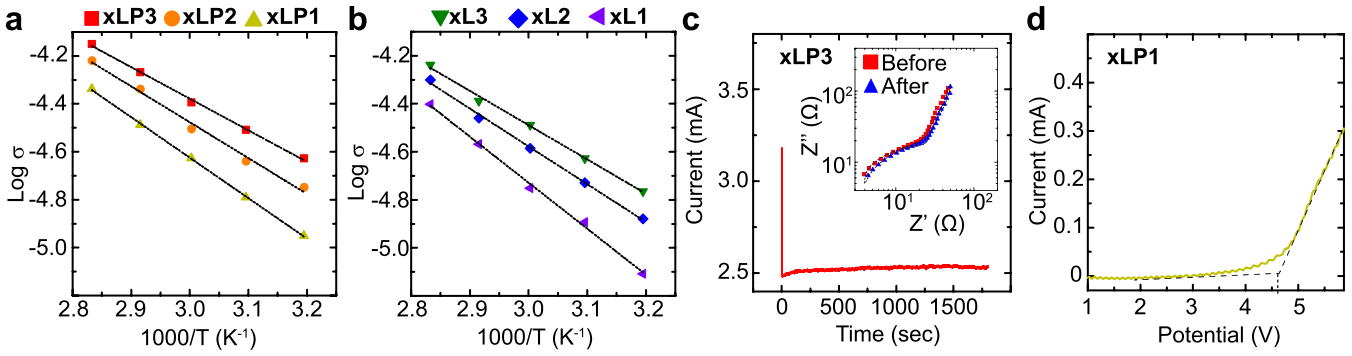

Figure 4. Electrochemical properties of xLs and xLPs. The change in ionic conductivity (ln σ) as a function of an inverse value of temperature (T) for (a) **xLP**s and (b) **xL**s. (c) Time-dependent current polarization profile of **xLP3**. The inset shows EIS spectra of **xLP3** before and after polarization. (d) Linear sweep voltammetry curve of **xLP1**.

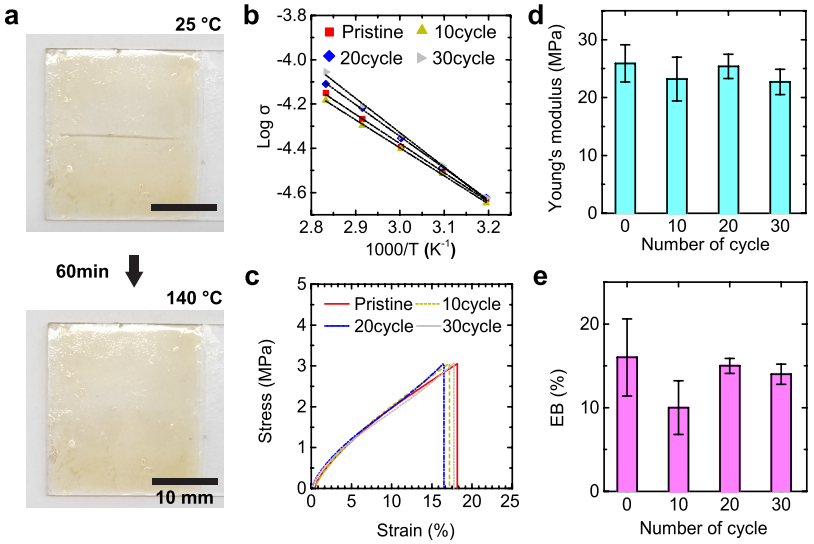

Figure 5. Mechanical and electrochemical properties of xLP3 after multiple reprocessing cycles. (a) Photograph of the scratched and self-healed **xLP3** film, which was coated on a glass by a solvent casting method. (b) Ionic conductivity of **xLP3** at different reprocessing cycles as a function of temperature. (c) Stress−strain curve of pristine and reprocessed **xLP3**. (d) Young's modulus and (e) elongation at break (EB) of **xLP3** with the number of reprocessing cycles. Reported values and error bars represent the average and one standard deviation, respectively.

diffusion of cross-linkers in the polymer matrix. Furthermore, the copolymer containing PEO showed a lower E_a value than the copolymer without PEO moieties at the same electrolyte ratio.

The engineering stress (σ) and strain (ε) responses of **xL**s and **xLP**s at room temperature were characterized under the application of uniaxial tension (Figures 3e,f, S11). Despite variations in their cross-linking density, both samples displayed a relatively brittle behavior, which can be attributed to the higher portion of P(LiSTFSI) with a high T_g. Our cross-linked polymers demonstrated a tensile strength of 3 MPa, which is comparable to poly(vinylene carbonate).[53] The elongation at break for our polymers ranged from 5 to 20%, similar to that of poly(benzimidazole) electrolytes.[11] Additionally, the brittleness increased with higher furan composition due to a decrease in the average chain length between cross-linking points.[54,55] When comparing the stress−strain behaviors of **xL**s with **xLP**s, we found that PEO units from PEGFMA did not significantly impact the mechanical properties, despite their low T_g. We assume that the mechanical properties of **xLP**s may be reinforced by the ion−dipole interaction between lithium ions and PEO units.[56,57]

3.4. Electrochemical Properties of xLs and xLPs. Ionic conductivity was determined by measuring the bulk resistance using electrochemical impedance spectroscopy (EIS) at different temperatures (Figures 4a,b, S12, Table S2). Both **xL**s and **xLP**s showed an increase in ionic conductivity as the electrolyte content increased, which can be attributed to the formation of well-connected ion conducting channels.[58,59] Furthermore, an increase in the electrolyte content leads to a decrease in the cross-linking part, which is beneficial for enhancing ion mobility due to the reduction in the T_g of the polymer.[60] Among the samples, **xL1** showed the lowest conductivity of 7.8×10^{-6} and 4.0×10^{-5} S cm^{-1} at 40 and 80 °C, respectively. On the other hand, **xLP3** exhibited the highest conductivity of 2.4×10^{-5} and 7.1×10^{-5} S cm^{-1} at 40 and 80 °C, respectively. We compared the ionic conductivity of our material with reported values from various sulfonylimide-type SPEs at similar temperature ranges. For instance, block copolymers composed of polysulfonyl imide and poly(PEGMA) exhibited an ionic conductivity of 1.0×10^{-5} S cm^{-1} at 80 °C,[61] while poly(ethylene oxide carbonate)-based TFSI random copolymers demonstrated an ionic conductivity of 2.9×10^{-5} S cm^{-1} at 70 °C.[62] Blending perfluorinated sulfonylimide polymers with polyethers resulted in 5×10^{-7} S

https://doi.org/10.1021/acsapm.3c01319
ACS Appl. Polym. Mater. 2023, 5, 7433−7442

cm^{-1} at 80 °C.[34] PLiSTFSI-*co*-PEGDMA, which shares similarities with our polymeric system, exhibited ionic conductivities ranging from 4.00×10^{-6} to 1.00×10^{-4} S cm^{-1} at 40−80 °C.[63] Hence, our polymer electrolytes demonstrate comparable ionic conducting abilities to previously reported systems. Interestingly, our polymer systems demonstrated a relatively higher ionic conductivity at low temperature ranges. We speculate that the bismaleimide cross-linkers have a positive influence on the ionic conductivity.[64]

The ionic conductivity of **xLP**s is higher compared to that of **xL**s at the same electrolyte content due to the facilitated mobility of lithium ions by PEO in the polymer matrix. This is supported by the activation energy values calculated from the Arrhenius plot. The values of E_a of **xLP3**, **xLP2**, and **xLP1** are 25.0, 28.9, and 32.8 kJ mol^{-1}, respectively, while for **xL3**, **xL2**, and **xL1**, the values are 27.0, 30.8, and 36.7 kJ mol^{-1}, respectively. Previous studies reported an E_a of 24.8 kJ mol^{-1} for a PLiSTFSI-PEGMA copolymer system,[65] which is comparable with our results.

The transference number of the lithium ion (t_{Li}^+) in the matrix was measured by using a polarization profile with EIS (Figures 4c, S13, Table S3). Having a high transference number is crucial for achieving improved performance during charging/discharging processes and minimizing concentration polarization.[66] Except for **xL1**, which displayed the lowest value of 0.75, all samples have a high t_{Li}^+ close to 1.0. This high value can be attributed to the immobilized anionic moieties, indicating a good performance as a single-ion conductor.[67] The electrochemical stability window (ESW) of each sample was measured by using LSV (Figure S14, Table S2). For **xLP1**, which exhibited the lowest ESW compared to other samples, there is no obvious anodic current peak until 4.6 V, demonstrating excellent electrochemical stability (Figure 4d). The ESW of the remaining samples ranges from 4.6 to 5.6 V.

3.5. Reprocessability of xLP3. Thermally reversible Diels−Alder chemistry enables our synthesized polymers to possess self-healing capabilities and reprocessability. Upon scratching the surface of **xLP3** with a sharp knife, the scratched region was fully healed through thermal treatment at 140 °C for 60 min (Figure 5a). Additionally, we conducted up to 30 cycles of thermal reprocessing with **xLP3** and assessed both their ionic conductivities and mechanical properties. Even after 30 cycles of thermal reprocessing, **xLP3** exhibited consistent conductivity values across different temperatures while maintaining their E_a within the range of 24−28.0 kJ mol^{-1} (Figure 5b). The tensile properties of reprocessed **xLP3** were measured using DMA (Figure 5c−e). We found that the differences in the stress−strain curves, Young's modulus, and elongation at break (EB) for each sample were not statistically significant. Toughness and yield stress showed no statistical difference as well (Figure S15).

4. CONCLUSIONS

We have successfully synthesized thermally reprocessable and self-healing polymer electrolytes by varying the chemical structures of furan-containing monomers and the proportion of electrolytic components. The formation of Diels−Alder adducts was confirmed by FT-IR, DSC, and the reversible change in solubility with temperature. The thermomechanical and tensile properties of the polymers were found to be significantly influenced by cross-linking density and the presence of PEG units in the comonomer. Due to their single-ion conducting nature, our copolymers exhibited a high transference number close to 1.0 with an excellent ionic conductivity of 7.07×10^{-5} S cm^{-1} at 80 °C. Even after undergoing up to 30 reprocessing cycles, these polymers maintained their good ion conductivity as well as mechanical properties. We envision that our self-healing and reprocessable thermosets hold great promise as solid polymer electrolytes for lithium-ion batteries, providing a safe and environmentally friendly approach.

■ ASSOCIATED CONTENT

Supporting Information

The Supporting Information is available free of charge at https://pubs.acs.org/doi/10.1021/acsapm.3c01319.

^{1}H and ^{13}C NMR of monomers; NMR, GPC, and TGA analysis of linear polymers; swelling tests, stress relaxation, and summarized mechanical properties of cross-linked polymers; EIS profile, ionic conductivities, polarization profiles, and linear sweep voltammetry curves of cross-linked polymers; and the change in the toughness and yield stress of **xLP3** after multiple recycling processes (PDF)

■ AUTHOR INFORMATION

Corresponding Authors

Jeong Gon Son − *KU-KIST Graduate School of Converging Science and Technology, Korea University, Seoul 02841, Republic of Korea; Soft Hybrid Materials Research Center, Korea Institute of Science and Technology, Seoul 02792, Republic of Korea;* orcid.org/0000-0003-3473-446X; Email: jgson@kist.re.kr

Tae Ann Kim − *Solutions to Electromagnetic Interference in Future-Mobility Research Center, Korea Institute of Science and Technology, Seoul 02792, Republic of Korea; Soft Hybrid Materials Research Center, Korea Institute of Science and Technology, Seoul 02792, Republic of Korea; Division of Energy & Environment Technology, KIST School, Korea University of Science and Technology (UST), Seoul 02792, Republic of Korea;* orcid.org/0000-0002-1084-638X; Email: takim717@kist.re.kr

Authors

Sangho Lee − *Solutions to Electromagnetic Interference in Future-Mobility Research Center, Korea Institute of Science and Technology, Seoul 02792, Republic of Korea*

Juhwan Song − *Solutions to Electromagnetic Interference in Future-Mobility Research Center, Korea Institute of Science and Technology, Seoul 02792, Republic of Korea; KU-KIST Graduate School of Converging Science and Technology, Korea University, Seoul 02841, Republic of Korea*

Jinhan Cho − *KU-KIST Graduate School of Converging Science and Technology and Department of Chemical and Biological Engineering, Korea University, Seoul 02841, Republic of Korea; Soft Hybrid Materials Research Center, Korea Institute of Science and Technology, Seoul 02792, Republic of Korea;* orcid.org/0000-0002-7097-5968

Complete contact information is available at: https://pubs.acs.org/10.1021/acsapm.3c01319

Author Contributions

#S.L. and J.S. contributed equally to this work. S.L., J.S., and T.A.K. conceived and planned the experiments. S.L. and J.S. performed the experiments. S.L., J.S., J.C., J.G.S., and T.A.K.

wrote the manuscript. All authors provided valuable feedback regarding data analysis and manuscript.

Notes

The authors declare no competing financial interest.

The authors declare no competing financial interest or personal relationships that could have appeared to influence the work reported in this paper.

■ ACKNOWLEDGMENTS

We gratefully acknowledge financial support from the Korea Institute of Science and Technology (KIST) Institutional Program and a National Research Council of Science & Technology (NST) grant from the Korean government (MSIT) (CRC22031-000).

■ REFERENCES

(1) Xu, R.; Zhang, X. Q.; Cheng, X. B.; Peng, H. J.; Zhao, C. Z.; Yan, C.; Huang, J. Q. Artificial Soft−Rigid Protective Layer for Dendrite-Free Lithium Metal Anode. *Adv. Funct. Mater.* **2018**, *28*, No. 1705838.

(2) Kim, Y. S. Polymer Electrolytes with High Ionic Concentration for Fuel Cells and Electrolyzers. In *ACS Applied Polymer Materials*; American Chemical Society, March 2021; Vol. *12*, pp 1250−1270 DOI: 10.1021/acsapm.0c01405.

(3) Haile, S. M.; Boysen, D. A.; Chisholm, C. R. I.; Merle, R.B. Solid Acids as Fuel Cell Electrolytes. *Nature* **2001**, *410*, 910−913.

(4) Freitas, F. S.; Freitas, J. N. D.; Ito, B. I.; Paoli, M. A. D.; Nogueira, A. F. Electrochemical and Structural Characterization of Polymer Gel Electrolytes Based on a PEO Copolymer and an Imidazolium-Based Ionic Liquid for Dye-Sensitized Solar Cells. *ACS Appl. Mater. Interfaces* **2009**, *1*, 2870−2877.

(5) Li, N.; Guiver, M. D. Ion Transport by Nanochannels in Ion-Containing Aromatic Copolymers. In *Macromolecules*; American Chemical Society, April 2014; Vol. *8*, pp 2175−2198 DOI: 10.1021/ma402254h.

(6) Wang, Y. Recent Research Progress on Polymer Electrolytes for Dye-Sensitized Solar Cells. *Sol. Energy Mater. Sol. Cells* **2009**, *93*, 1167−1175.

(7) Di Noto, V.; Lavina, S.; Giffin, G. A.; Negro, E.; Scrosati, B. Polymer Electrolytes: Present, Past and Future. In *Electrochim. Acta*; Elsevier Ltd., 2011; Vol. *57*, pp 4−13 DOI: 10.1016/j.electacta.2011.08.048.

(8) Deng, K.; Zeng, Q.; Wang, D.; Liu, Z.; Qiu, Z.; Zhang, Y.; Xiao, M.; Meng, Y. Single-Ion Conducting Gel Polymer Electrolytes: Design, Preparation and Application. *J. Mater. Chem. A* **2020**, *8*, 1557−1577.

(9) Gao, J.; Wang, C.; Han, D. W.; Shin, D. M. Single-Ion Conducting Polymer Electrolytes as a Key Jigsaw Piece for next-Generation Battery Applications. *Chem. Sci.* **2021**, *12*, 13248−13272.

(10) Zhang, H.; Li, C.; Eshetu, G. G.; Laruelle, S.; Grugeon, S.; Zaghib, K.; Julien, C.; Mauger, A.; Guyomard, D.; Rojo, T.; Gisbert-Trejo, N.; Passerini, S.; Huang, X.; Zhou, Z.; Johansson, P.; Forsyth, M. From Solid-Solution Electrodes and the Rocking-Chair Concept to Today's Batteries. *Angew. Chem.* **2020**, *132*, 542−546.

(11) Du, D.; Li, H.; Xu, H.; Zhang, Y.; Sun, Y.; Zeng, D.; Cheng, H. Lithium Propanesulfonyl(Trifluoromethylsulfonyl)Imide Grafted Polybenzimidazole as a Self-Supporting Single Ion Conducting Polymer Electrolyte Membrane for Lithium Metal Secondary Batteries. *J. Alloys Compd.* **2021**, *881*, 160573.

(12) Jangu, C.; Savage, A. M.; Zhang, Z.; Schultz, A. R.; Madsen, L. A.; Beyer, F. L.; Long, T. E. Sulfonimide-Containing Triblock Copolymers for Improved Conductivity and Mechanical Performance. *Macromolecules* **2015**, *48*, 4520−4528.

(13) Fan, L. Z.; He, H.; Nan, C. W. Tailoring Inorganic−Polymer Composites for the Mass Production of Solid-State Batteries. *Nat. Rev. Mater.* **2021**, *6*, 1003−1019.

(14) Lin, Y.; Chen, Y.; Yu, Z.; Huang, Z.; Lai, J. C.; Tok, J. B. H.; Cui, Y.; Bao, Z. Reprocessable and Recyclable Polymer Network Electrolytes via Incorporation of Dynamic Covalent Bonds. *Chem. Mater.* **2022**, *34*, 2393−2399.

(15) Liao, H.; Zhong, W.; Li, T.; Han, J.; Sun, X.; Tong, X.; Zhang, Y. A Review of Self-Healing Electrolyte and Their Applications in Flexible/Stretchable Energy Storage Devices. *Electrochim. Acta* **2022**, *404*, No. 139730.

(16) Wan, L.; Cao, X.; Xue, X.; Tong, Y.; Ci, S.; Huang, H.; Zhou, D. Self-Healing and Flexible Ionic Gel Polymer Electrolyte Based on Reversible Bond for High-Performance Lithium Metal Batteries. *Energy Technol.* **2022**, *10*, No. 2100749.

(17) Chakma, P.; Konkolewicz, D. Dynamic Covalent Bonds in Polymeric Materials. *Angew. Chem., Int. Ed.* **2019**, *58*, 9682−9695.

(18) Elling, B. R.; Dichtel, W. R. Reprocessable Cross-Linked Polymer Networks: Are Associative Exchange Mechanisms Desirable? *ACS Cent. Sci.* **2020**, *6*, 1488−1496.

(19) Huang, Z. X.; Xie, Z. H.; Zhang, Z. P.; Zhang, T.; Rong, M. Z.; Zhang, M. Q. Highly Ionic Conductive, Self-Healable Solid Polymer Electrolyte Based on Reversibly Interlocked Macromolecule Networks for Lithium Metal Batteries Workable at Room Temperature. *J. Mater. Chem. A* **2022**, *10*, 18895−18906.

(20) Lee, Y.; Kim, M.; Kim, H.; Lee, K. H.; Kim, S. Self-Healable and Tough Polymer Electrolyte Composites Based on Associative Nanostructural Networks. *ACS Appl. Polym. Mater.* **2022**, *4*, 5821−5830.

(21) Cho, D. H.; Cho, K. G.; An, S.; Kim, M. S.; Oh, H. W.; Yeo, J.; Yoo, W. C.; Hong, K.; Kim, M.; Lee, K. H. Self-Healable, Stretchable, and Nonvolatile Solid Polymer Electrolytes for Sustainable Energy Storage and Sensing Applications. *Energy Storage Mater.* **2022**, *45*, 323−331.

(22) Meyer, W. H. Polymer Electrolytes for Lithium-Ion Batteries. *Adv. Mater.* **1998**, *10*, 439−448.

(23) Marinow, A.; Katcharava, Z.; Binder, W. H. Self-Healing Polymer Electrolytes for Next-Generation Lithium Batteries. *Polymers* **2023**, *15*, 1145.

(24) Gorecki, W.; Jeannin, M.; Belorizky, E.; Roux, C.; Armand, M. Physical Properties of Solid Polymer Electrolyte PEO(LiTFSI) Complexes. *J. Phys.: Condens. Matter* **1995**, *7*, 6823.

(25) Tong, B.; Song, Z.; Wu, H.; Wang, X.; Feng, W.; Zhou, Z.; Zhang, H. Ion Transport and Structural Design of Lithium-Ion Conductive Solid Polymer Electrolytes: A Perspective. *Mater. Futures* **2022**, *1*, No. 042103.

(26) Zhao, S.; Zhang, Y.; Pham, H.; Carrillo, J. M. Y.; Sumpter, B. G.; Nanda, J.; Dudney, N. J.; Saito, T.; Sokolov, A. P.; Cao, P. F. Improved Single-Ion Conductivity of Polymer Electrolyte via Accelerated Segmental Dynamics. *ACS Appl. Energy Mater.* **2020**, *3*, 12540−12548.

(27) Liu, D.; Yang, W.; Liu, Y.; Yang, S.; Shen, Z.; Fan, X. H.; Yang, H.; Zhou, Q. F. Enhancing Ionic Conductivity in Tablet-Bottlebrush Block Copolymer Electrolytes with Well-Aligned Nanostructures via Solvent Vapor Annealing†. *J. Mater. Chem. C* **2022**, *10*, 4247−4256.

(28) Wu, F.; Luo, L.; Tang, Z.; Liu, D.; Shen, Z.; Fan, X. H. Block Copolymer Electrolytes with Excellent Properties in a Wide Temperature Range. *ACS Appl. Energy Mater.* **2020**, *3*, 6536−6543.

(29) Yuan, H.; Luan, J.; Yang, Z.; Zhang, J.; Wu, Y.; Lu, Z.; Liu, H. Single Lithium-Ion Conducting Solid Polymer Electrolyte with Superior Electrochemical Stability and Interfacial Compatibility for Solid-State Lithium Metal Batteries. *ACS Appl. Mater. Interfaces* **2020**, *12*, 7249−7256.

(30) Ma, Q.; Zhang, H.; Zhou, C.; Zheng, L.; Cheng, P.; Nie, J.; Feng, W.; Hu, Y.-S.; Li, H.; Huang, X.; Chen, L.; Armand, M.; Zhou, Z. Single Lithium-Ion Conducting Polymer Electrolytes Based on a Super-Delocalized Polyanion. *Angew. Chem.* **2016**, *128*, 2567−2571.

(31) Martinez-Ibañez, M.; Sanchez-Diez, E.; Qiao, L.; Zhang, Y.; Judez, X.; Santiago, A.; Aldalur, I.; Carrasco, J.; Zhu, H.; Forsyth, M.; Armand, M.; Zhang, H. Unprecedented Improvement of Single Li-Ion Conductive Solid Polymer Electrolyte Through Salt Additive. *Adv. Funct. Mater.* **2020**, *30*, 2000455.

(32) Zhang, H.; Li, C.; Piszcz, M.; Coya, E.; Rojo, T.; Rodriguez-Martinez, L. M.; Armand, M.; Zhou, Z. Single Lithium-Ion

Conducting Solid Polymer Electrolytes: Advances and Perspectives. In *Chemical Society Reviews*; Royal Society of Chemistry, February 2017; Vol. 7, pp 797−815 DOI: 10.1039/c6cs00491a.
(33) Jia, Z.; Yuan, W.; Sheng, C.; Zhao, H.; Hu, H.; Baker, G. L. Optimizing the Electrochemical Performance of Imidazolium-Based Polymeric Ionic Liquids by Varying Tethering Groups. *J. Polym. Sci., Part A: Polym. Chem.* **2015**, *53*, 1339−1350.
(34) Watanabe, M.; Suzuki, Y.; Nishimoto, A. *Single Ion Conduction in Polyether Electrolytes Alloyed with Lithium Salt of a Perfluorinated Polyimide*; 2000, Vol. *45*. www.elsevier.nl/locate/electacta.
(35) Martinez-Ibañez, M.; Sanchez-Diez, E.; Qiao, L.; Meabe, L.; Santiago, A.; Zhu, H.; O'Dell, L. A.; Carrasco, J.; Forsyth, M.; Armand, M.; Zhang, H. Weakly Coordinating Fluorine-Free Polysalt for Single Lithium-Ion Conductive Solid Polymer Electrolytes. *Batteries Supercaps* **2020**, *3*, 738−746.
(36) Meziane, R.; Bonnet, J. P.; Courty, M.; Djellab, K.; Armand, M. Single-Ion Polymer Electrolytes Based on a Delocalized Polyanion for Lithium Batteries. In *Electrochim. Acta*; Elsevier Ltd., 2011; Vol. *57*, pp 14−19 DOI: 10.1016/j.electacta.2011.03.074.
(37) Lee, H. Y.; Cha, S. H. Enhancement of Self-Healing Property by Introducing Ethylene Glycol Group into Thermally Reversible Diels-Alder Reaction Based Self-Healable Materials. *Macromol. Res.* **2017**, *25*, 640−647.
(38) Yoon, S.; Choi, J. H.; Sung, B. J.; Bang, J.; Kim, T. A. Mechanochromic and Thermally Reprocessable Thermosets for Autonomic Damage Reporting and Self-Healing Coatings. *NPG Asia Mater.* **2022**, *14*, No. 61.
(39) Abraham, K. M.; Jiang, Z.; Carroll, B. Highly Conductive PEO-like Polymer Electrolytes. *Chem. Mater.* **1997**, *9*, 1978−1988.
(40) Peniche, C.; Zaldivar, D.; Bulay, A.; Rom∼in, J. S. *Study of the Thermal Degradation of Poly(Furfuryi Methacrylate) by Thermogravimetry*; 1993, Vol. *40*.
(41) Postiglione, G.; Turri, S.; Levi, M. Effect of the Plasticizer on the Self-Healing Properties of a Polymer Coating Based on the Thermoreversible Diels-Alder Reaction. In *Progress in Organic Coatings*; Elsevier B.V., 2015; Vol. *78*, pp 526−531 DOI: 10.1016/j.porgcoat.2014.05.022.
(42) Froidevaux, V.; Borne, M.; Laborbe, E.; Auvergne, R.; Gandini, A.; Boutevin, B. Study of the Diels-Alder and Retro-Diels-Alder Reaction between Furan Derivatives and Maleimide for the Creation of New Materials. *RSC Adv.* **2015**, *5*, 37742−37754.
(43) de Oliveira, J. C.; Laborie, M. P.; Roucoules, V. Thermodynamic and Kinetic Study of Diels−Alder Reaction between Furfuryl Alcohol and N-Hydroxymaleimides — An Assessment for Materials Application. *Molecules* **2020**, *25*, 243.
(44) Chen, X.; Li, L.; Torkelson, J. M. Recyclable Polymer Networks Containing Hydroxyurethane Dynamic Cross-Links: Tuning Morphology, Cross-Link Density, and Associated Properties with Chain Extenders. *Polymer* **2019**, *178*, 121604.
(45) Ma, S.; Jiang, M.; Tao, P.; Song, C.; Wu, J.; Wang, J.; Deng, T.; Shang, W. Temperature Effect and Thermal Impact in Lithium-Ion Batteries: A Review. In *Progress in Natural Science: Materials International*; Elsevier B.V., December 2018; Vol. *1*, pp 653−666 DOI: 10.1016/j.pnsc.2018.11.002.
(46) Khurana, R.; Schaefer, J. L.; Archer, L. A.; Coates, G. W. Suppression of Lithium Dendrite Growth Using Cross-Linked Polyethylene/Poly(Ethylene Oxide) Electrolytes: A New Approach for Practical Lithium-Metal Polymer Batteries. *J. Am. Chem. Soc.* **2014**, *136*, 7395−7402.
(47) Monroe, C.; Newman, J. The Impact of Elastic Deformation on Deposition Kinetics at Lithium/Polymer Interfaces. *J. Electrochem. Soc.* **2005**, *152*, A396.
(48) Glynos, E.; Pantazidis, C.; Sakellariou, G. Designing All-Polymer Nanostructured Solid Electrolytes: Advances and Prospects. *ACS Omega* **2020**, *5*, 2531−2540.
(49) Liu, J.; Pickett, P. D.; Park, B.; Upadhyay, S. P.; Orski, S. V.; Schaefer, J. L. Non-Solvating, Side-Chain Polymer Electrolytes as Lithium Single-Ion Conductors: Synthesis and Ion Transport Characterization. *Polym Chem* **2020**, *11*, 461−471.
(50) Guzmán, G.; Nava, D. P.; Vazquez-Arenas, J.; Cardoso, J. Design of a Zwitterion Polymer Electrolyte Based on Poly[Poly (Ethylene Glycol) Methacrylate]: The Effect of Sulfobetaine Group on Thermal Properties and Ionic Conduction. *Macromol. Symp.* **2017**, *374*, No. 1600136.
(51) Feng, S. K.; Schmitt, M.; Chen, E. Y. X. Organocatalytic Polymerization of Furfuryl Methacrylate and Post-Diels-Alder Click Reaction to Cross-Linked Materials. *Macromol. Chem. Phys.* **2015**, *216*, 1421−1430.
(52) Orozco, F.; Li, J.; Ezekiel, U.; Niyazov, Z.; Floyd, L.; Lima, G. M. R.; Winkelman, J. G. M.; Moreno-Villoslada, I.; Picchioni, F.; Bose, R. K. Diels-Alder-Based Thermo-Reversibly Crosslinked Polymers: Interplay of Crosslinking Density, Network Mobility, Kinetics and Stereoisomerism. *Eur. Polym. J.* **2020**, *135*, No. 109882.
(53) Shan, X.; Zhao, S.; Ma, M.; Pan, Y.; Xiao, Z.; Li, B.; Sokolov, A. P.; Tian, M.; Yang, H.; Cao, P. F. Single-Ion Conducting Polymeric Protective Interlayer for Stable Solid Lithium-Metal Batteries. *ACS Appl. Mater. Interfaces* **2022**, *14*, 56110−56119.
(54) Boden, J.; Bowen, C. R.; Buchard, A.; Davidson, M. G.; Norris, C. Understanding the Effects of Cross-Linking Density on the Self-Healing Performance of Epoxidized Natural Rubber and Natural Rubber. *ACS Omega* **2022**, *7*, 15098−15105.
(55) Buehler, M. J. Nanomechanics of Collagen Fibrils under Varying Cross-Link Densities: Atomistic and Continuum Studies. *J. Mech. Behav. Biomed. Mater.* **2008**, *1*, 59−67.
(56) Ding, W. Q.; Lv, F.; Xu, N.; Wu, M. T.; Liu, J.; Gao, X. P. Polyethylene Oxide-Based Solid-State Composite Polymer Electrolytes for Rechargeable Lithium Batteries. *ACS Appl Energy Mater.* **2021**, *4*, 4581−4601.
(57) Feng, J.; Wang, L.; Chen, Y.; Wang, P.; Zhang, H.; He, X. PEO Based Polymer-Ceramic Hybrid Solid Electrolytes: A Review. In *Nano Convergence*; Korea Nano Technology Research Society, December 2021; Vol. *1* DOI: 10.1186/s40580-020-00252-5.
(58) Xu, L.; Li, J.; Deng, W.; Li, L.; Zou, G.; Hou, H.; Huang, L.; Ji, X. Boosting the Ionic Conductivity of PEO Electrolytes by Waste Eggshell-Derived Fillers for High-Performance Solid Lithium/Sodium Batteries. In *Materials Chemistry Frontiers*; Royal Society of Chemistry, February 2021; Vol. *7*, pp 1315−1323 DOI: 10.1039/d0qm00541j.
(59) Olmedo-Martínez, J.; Meabe, L.; Basterretxea, A.; Mecerreyes, D.; Müller, A. J. Effect of Chemical Structure and Salt Concentration on the Crystallization and Ionic Conductivity of Aliphatic Polyethers. *Polymers* **2019**, *11*, No. 452.
(60) Shen, C.; Zhao, Q.; Shan, N.; Jing, B. B.; Evans, C. M. Conductivity−Modulus− T g Relationships in Solvent-free, Single Lithium Ion Conducting Network Electrolytes. *J. Polym. Sci.* **2020**, *58*, 2376−2388.
(61) Porcarelli, L.; Shaplov, A. S.; Salsamendi, M.; Nair, J. R.; Vygodskii, Y. S.; Mecerreyes, D.; Gerbaldi, C. Single-Ion Block Copoly(Ionic Liquid)s as Electrolytes for All-Solid State Lithium Batteries. *ACS Appl. Mater. Interfaces* **2016**, *8*, 10350−10359.
(62) Meabe, L.; Goujon, N.; Li, C.; Armand, M.; Forsyth, M.; Mecerreyes, D. Single-Ion Conducting Poly(Ethylene Oxide Carbonate) as Solid Polymer Electrolyte for Lithium Batteries. *Batteries Supercaps* **2020**, *3*, 68−75.
(63) Feng, S.; Shi, D.; Liu, F.; Zheng, L.; Nie, J.; Feng, W.; Huang, X.; Armand, M.; Zhou, Z. Single Lithium-Ion Conducting Polymer Electrolytes Based on Poly[(4-Styrenesulfonyl)-(Trifluoromethanesulfonyl)Imide] Anions. *Electrochim. Acta* **2013**, *93*, 254−263.
(64) Ping, J.; Pan, Y.; Pan, H.; Wu, B.; Zhou, H.; Shen, Z.; Fan, X. H. Microphase Separation and High Ionic Conductivity at High Temperatures of Lithium Salt-Doped Amphiphilic Alternating Copolymer Brush with Rigid Side Chains. *Macromolecules* **2015**, *48*, 8557−8564.
(65) Tu, Z.; Kambe, Y.; Lu, Y.; Archer, L. A. Nanoporous Polymer-Ceramic Composite Electrolytes for Lithium Metal Batteries. *Adv. Energy Mater.* **2014**, *4*, No. 1300654.

(66) Li, Y.; Wong, K. W.; Dou, Q.; Ng, K. M. A Single-Ion Conducting and Shear-Thinning Polymer Electrolyte Based on Ionic Liquid-Decorated PMMA Nanoparticles for Lithium-Metal Batteries. *J. Mater. Chem. A* **2016**, *4*, 18543−18550.
(67) Zhou, D.; Tkacheva, A.; Tang, X.; Sun, B.; Shanmukaraj, D.; Li, P.; Zhang, F.; Armand, M.; Wang, G. Stable Conversion Chemistry-Based Lithium Metal Batteries Enabled by Hierarchical Multifunctional Polymer Electrolytes with Near-Single Ion Conduction. *Angew. Chem.* **2019**, *131*, 6062−6067.

https://doi.org/10.1021/acsapm.3c01319
ACS Appl. Polym. Mater. 2023, 5, 7433−7442